NASA/TM—2004-213355 AIAA–2004–5700

Unitized Regenerative Fuel Cell System Gas Dryer/Humidifier Analytical Model Development

Kenneth A. Burke
Glenn Research Center, Cleveland, Ohio

Ian Jakupca
Analex Corporation, Brook Park, Ohio

October 2004

The NASA STI Program Office . . . in Profile

Since its founding, NASA has been dedicated to the advancement of aeronautics and space science. The NASA Scientific and Technical Information (STI) Program Office plays a key part in helping NASA maintain this important role.

The NASA STI Program Office is operated by Langley Research Center, the Lead Center for NASA's scientific and technical information. The NASA STI Program Office provides access to the NASA STI Database, the largest collection of aeronautical and space science STI in the world. The Program Office is also NASA's institutional mechanism for disseminating the results of its research and development activities. These results are published by NASA in the NASA STI Report Series, which includes the following report types:

- TECHNICAL PUBLICATION. Reports of completed research or a major significant phase of research that present the results of NASA programs and include extensive data or theoretical analysis. Includes compilations of significant scientific and technical data and information deemed to be of continuing reference value. NASA's counterpart of peer-reviewed formal professional papers but has less stringent limitations on manuscript length and extent of graphic presentations.

- TECHNICAL MEMORANDUM. Scientific and technical findings that are preliminary or of specialized interest, e.g., quick release reports, working papers, and bibliographies that contain minimal annotation. Does not contain extensive analysis.

- CONTRACTOR REPORT. Scientific and technical findings by NASA-sponsored contractors and grantees.

- CONFERENCE PUBLICATION. Collected papers from scientific and technical conferences, symposia, seminars, or other meetings sponsored or cosponsored by NASA.

- SPECIAL PUBLICATION. Scientific, technical, or historical information from NASA programs, projects, and missions, often concerned with subjects having substantial public interest.

- TECHNICAL TRANSLATION. English-language translations of foreign scientific and technical material pertinent to NASA's mission.

Specialized services that complement the STI Program Office's diverse offerings include creating custom thesauri, building customized databases, organizing and publishing research results . . . even providing videos.

For more information about the NASA STI Program Office, see the following:

- Access the NASA STI Program Home Page at ***http://www.sti.nasa.gov***

- E-mail your question via the Internet to help@sti.nasa.gov

- Fax your question to the NASA Access Help Desk at 301–621–0134

- Telephone the NASA Access Help Desk at 301–621–0390

- Write to:
  NASA Access Help Desk
  NASA Center for AeroSpace Information
  7121 Standard Drive
  Hanover, MD 21076

NASA/TM—2004-213355 AIAA–2004–5700

Unitized Regenerative Fuel Cell System Gas Dryer/Humidifier Analytical Model Development

Kenneth A. Burke
Glenn Research Center, Cleveland, Ohio

Ian Jakupca
Analex Corporation, Brook Park, Ohio

Prepared for the
Second International Energy Conversion Engineering Conference
sponsored by the American Institute of Aeronautics and Astronautics
Providence, Rhode Island, August 16–19, 2004

National Aeronautics and
Space Administration

Glenn Research Center

October 2004

Available from

NASA Center for Aerospace Information
7121 Standard Drive
Hanover, MD 21076

National Technical Information Service
5285 Port Royal Road
Springfield, VA 22100

Available electronically at http://gltrs.grc.nasa.gov

Unitized Regenerative Fuel Cell System Gas Dryer/Humidifier Analytical Model Development

Kenneth A. Burke
National Aeronautics and Space Administration
Glenn Research Center
Cleveland, Ohio 44135

Ian Jakupca
Analex Corporation
Brook Park, Ohio 44135

Abstract

A lightweight Unitized Regenerative Fuel Cell (URFC) Energy Storage System concept is being developed at the NASA Glenn Research Center (GRC). This Unitized Regenerative Fuel Cell System (URFCS) is unique in that it uses Regenerative Gas Dryers/Humidifiers (RGD/H) that are mounted on the surface of the gas storage tanks that act as the radiators for thermal control of the Unitized Regenerative Fuel Cell System (URFCS). As the gas storage tanks cool down during URFCS charging the RGD/H dry the hydrogen and oxygen gases produced by electrolysis. As the gas storage tanks heat up during URFCS discharging, the RGD/H humidify the hydrogen and oxygen gases used by the fuel cell.

An analytical model was developed to simulate the URFCS RGD/H. The model is in the form of a Microsoft® Excel worksheet that allows the investigation of the RGD/H performance. Finite Element Analysis (FEA) modeling of the RGD/H and the gas storage tank wall was also done to analyze spatial temperature distribution within the RGD/H and the localized tank wall. Test results obtained from the testing of the RGD/H in a thermal vacuum environment were used to corroborate the analyses.

Introduction

The NASA Glenn Research Center Energetics Research Program is funding the development of a URFCS that will use a URFC as the main component of a lightweight, compact energy storage system. The goal of this program is to demonstrate the feasibility of a URFC energy storage system that can achieve an energy density of >400 W-h per kg of mass. While the program does not have the funding to produce actual flight weight hardware, enough development and testing will be completed such that the >400 W-h per kg goal can be confidently projected. To achieve this goal an innovative system concept was conceived and was the subject material of an earlier paper [1]. Ancillary components supporting this system concept, as well as supporting other fuel cell and electrolysis systems are being developed.

During the URFCS operation gases are produced which contain water vapor. Since the URFCS is envisioned to operate in extremely cold environment like high altitude airflight, space or Lunar or Martian surfaces, this water vapor will condense and freeze inside the gas storage tanks as well as inside the lines between the URFC stack and the gas storage tanks. To prevent this, there are two basic options.

The first option is to maintain the wetted gas storage surfaces above the dewpoint of the gas/water vapor mixtures. Since the dewpoint is typically above 50°C, this option requires the application of substantial insulation and energy. This results in added mass for insulation as well as larger tanks because of the higher gas storage temperature. Typically, there is also added parasitic power to energize trace heaters used to prevent condensation and freezing.

The second option is to dry the gases prior to their storage. This eliminates the need for line and tank insulation as well as parasitic power for trace heaters. The gas storage tanks can be smaller and lighter since the gas is stored cold. The challenge with this option is to dry the gases in a way that allows the water to be recovered and recycled by the URFCS. The RGD/H that was developed is able to do this function simply and effectively.

Background

As an energy storage system, the Regenerative Fuel Cell System (RFCS) "charges" and "discharges" like a rechargeable battery. A more detailed comparison of the RFCS to batteries has been described in an earlier paper [2]. While charging, the RFCS operates the electrolysis process, splitting water into hydrogen and oxygen. While discharging, the RFCS operates the fuel cell process, which combines hydrogen and oxygen and produces electricity and water

The key advantage of the URFCS over the RFCS is that the URFCS has a single cell stack that does both the process of electrolysis of water as well as the process of recombining of the hydrogen and oxygen gas to produce electricity. Since only one cell stack is needed instead of one electrolysis cell

stack and one fuel cell stack, a substantial amount of mass is saved because the cell stacks are major mass components of a RFCS. Besides saving the mass of one cell stack, the plumbing, wiring, structural mounting and ancillary equipment for one cell stack are also eliminated.

Figure 1 shows a schematic of a URFCS concept being developed at the NASA GRC. The system consists of the URFC stack, a gas storage system, pressure controls between the URFC stack and the gas storage system, a water storage tank, a heat pipe thermal control system, and a power/system control interface. A detailed description of the operating principles of this system has previously been described [1].

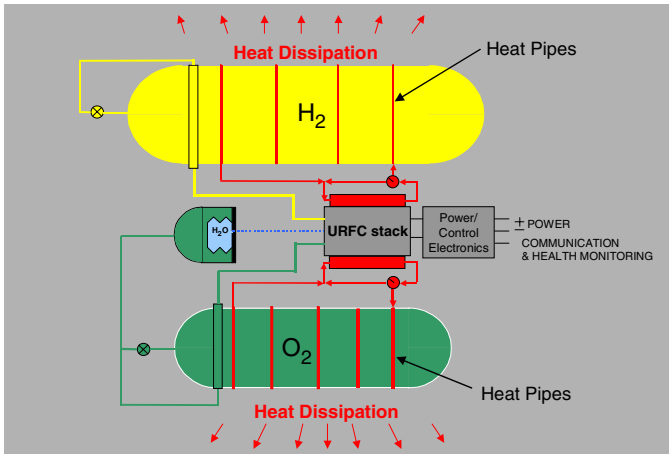

Figure 1.—URFC Schematic.

One of the aspects of the design concept shown in Figure 1 is the use of a section of tubing that is wrapped around the outside of each of the gas storage tanks. The gas storage tanks are also used as heat dissipation surfaces, and as the URFCS cycles between charging and discharging their surface temperatures cycle between freezing and thawing temperatures as described in an earlier paper [1]. Figure 2 is a plot of the surface temperature of the gas storage tanks as the URFCS charges and discharges. The expected charge efficiency during the URFCS charging is between 80 and 100%. At this efficiency, the surface of the gas storage tanks has an estimated steady state temperature between 73 and 245K. The expected discharge efficiency during the URFCS discharging is between 40 and 60%. At this efficiency, the surface of the gas storage tanks has an estimated steady state temperature between 300 and 331K. During the transitions between charging and discharging the tanks surface temperature will transition between these two temperature ranges. The quickness of this transition will depend on the specific heat and mass of the tanks.

The freeze-thaw cycle of the gas storage tanks is what allows the RGD/H to dry the oxygen and hydrogen during the URFCS charging by condensing and freezing the moisture within these gas streams, and then during URFCS discharging, to thaw the trapped ice and allow the oxygen and hydrogen to evaporate the moisture. This clears the moisture from the RGD/H and humidifies the gases prior to their entry into the URFC stack.

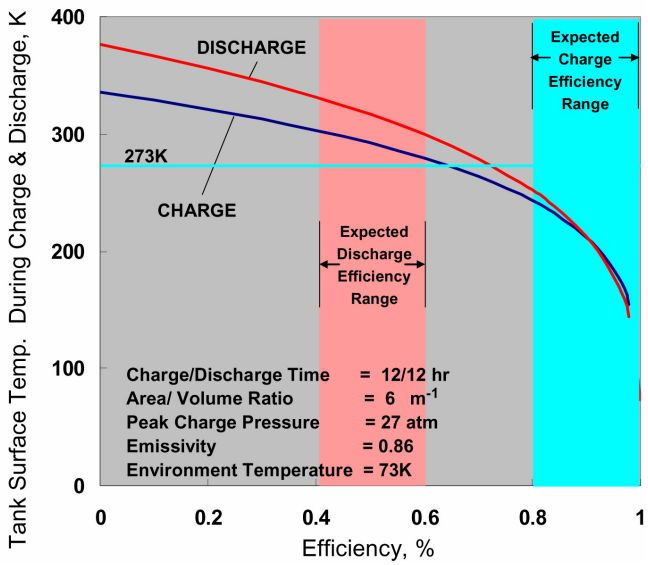

Figure 2.–Tank Surface Temperature vs. Efficiency.

There are many advantages of this approach. First is that it is extremely simple and rugged - a single section of piping adhered to the outside of the storage tank. This should maximize its durability and reliability. Another advantage is there is a minimum of components (only one), so that mass and volume are minimized. Still another advantage is that no parasitic power is required which increases system energy efficiency. Lastly there are no complicated control schemes for temperature maintenance of the condensing surface or the re-humidification of the product gases.

Analytical Model Description and Development

An analytical model was developed using Microsoft® Excel. The model was developed to analyze the de-humidification and re-humidification process occurring within the RGD/H. The model was also developed to obtain initial sizing estimates for the dryer test articles that were tested.

The RGD/H was modeled as a series of short individual sections of tubing as shown in Figure 3. The position of the first section was defined as the section which the warm, moist product gas leaving the URFC stack during the charging process (electrolysis) first enters as shown in Figure 3.

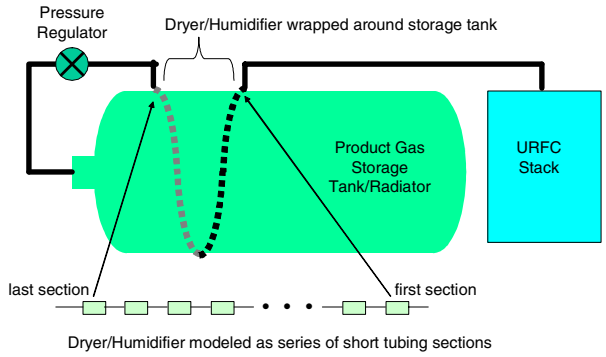

Figure 3.—Analytical Model.

Certain conditions are defined as inputs to the model of each short section of tubing. Based on these inputs, conditions at the section inlet and outlet are calculated. The following discussion describes the details of these calculations.

The following parameters are given as input to initiate the calculations for each short section. The index, i, refers to the inlet of the "ith" short section. The outlet from the "ith" section is the inlet to the "i + 1" section.

X_i = Length to inlet of ith section, cm (1)

D_i = Hydraulic diameter of ith section, cm (2)

ΔX = Length of section, cm (3)

T_i = Inlet flow temperature of ith section, K (4)

P_i = Inlet pressure of ith section, kPa (5)

$\frac{\partial m_{g,i}}{\partial t}$ = Inlet "dry gas" mass rate to ith section, kg/h (6)

S_i = Wall surface temperature of ith section, K (7)

The pressure is assumed to be constant along the length of the RGD/H. Even though the pressure drops along the length of the RGD/H due to viscous forces, this pressure drop is small enough that its effect on the calculated results is negligible.

The wall surface temperature for each section of the RGD/H is an input to the model. These values are experimentally determined or derived from the Finite Element Analysis (FEA) of the integrated assembly of the RGD/H and the heat rejection surface to which the RGD/H is attached.

Based on equations (1) through (7), and assuming that water vapor saturation conditions are always present (i.e. 100% relative humidity), the following inlet and outlet conditions are calculated.

The inlet partial pressure of water vapor at saturated conditions is a function of the inlet temperature. A Microsoft ® Excel formula was written that outputs the water vapor pressure for a given inlet temperature. This formula was developed using water vapor pressure versus temperature data from reference [3].

$$p_{w,i} = f_1(T_i) \quad (8)$$

The partial pressure of the product gas is then calculated by,

$$p_{g,i} = P_i - p_{w,i} \quad (9)$$

Where

$p_{w,i}$ = Inlet partial pressure of water vapor, kPa

$p_{g,i}$ = Inlet partial pressure of product gas, kPa

These partial pressures are then used to calculate the inlet mole fractions.

$$Y_{w,i} = (p_{w,i})/P_i \quad (10)$$

$$Y_{g,i} = (p_{g,i})/P_i \quad (11)$$

Where

$Y_{w,i}$ = Inlet mole fraction of water vapor, %

$Y_{g,i}$ = Inlet mole fraction of product gas, %

The inlet mass flow rate of water vapor is then calculated by,

$$\frac{\partial m_{w,i}}{\partial t} = \frac{\partial m_{g,i}}{\partial t} * M_g^{-1} * (Y_{w,i}/Y_{g,i}) * M_w \quad (12)$$

Where

$\frac{\partial m_{w,i}}{\partial t}$ = Inlet water vapor mass flow rate, kg/h

M_g = Molecular mass of the product gas, g/gmole

M_w = Molecular mass of water, g/gmole

The inlet total mass flow rate is then calculated by,

$$\frac{\partial m_i}{\partial t} = \frac{\partial m_{w,i}}{\partial t} + \frac{\partial m_{g,i}}{\partial t} \quad (13)$$

Where

$\frac{\partial m_i}{\partial t}$ = Inlet total mass flow rate, kg/h

The inlet vapor mixture density is calculated by,

$$\rho_i = \frac{(p_{g,i} M_g) + (p_{w,i} M_w)}{R T_i} \quad (14)$$

Where

ρ_i = Inlet vapor mixture density, kg/m^3

R = 8.3145 Joule-$gmole^{-1}$- K^{-1}

The inlet volumetric flow rate is then calculated by,

$$\frac{\partial V_i}{\partial t} = \frac{\partial m_i}{\partial t} * \rho_i^{-1} \quad (15)$$

Where

$\frac{\partial V_i}{\partial t}$ = Inlet volumetric flow rate, m^3/h

The flow channel cross-sectional area is calculated by,

$$A_i = \pi D_i^2 / 4 \quad (16)$$

and the inlet flow velocity is then calculated by,

$$\sigma_i = \frac{\partial V_i}{\partial t} A_i^{-1} * (10000 cm^3/m^3) \quad (17)$$

Where

A_i = Cross-sectional area, cm^2

σ_i = Inlet flow velocity of ith section, m/h

The inlet flow viscosity, the inlet flow kinematic viscosity, the inlet flow heat capacity, and the inlet flow thermal conductivity are functions of the type of product gas, the inlet pressure and inlet temperature. Four Microsoft® Excel formulas were written, one for each of these parameters. These formulas were developed using gas viscosity, kinematic viscosity, heat capacity, and thermal conductivity data from references [4] and [5].

$$\mu_i = f_2(\text{product gas}, P_i, T_i) \quad (18)$$
$$\nu_i = f_3(\text{product gas}, P_i, T_i) \quad (19)$$
$$C_{p,i} = f_4(\text{product gas}, P_i, T_i) \quad (20)$$
$$\lambda_i = f_5(\text{product gas}, P_i, T_i) \quad (21)$$

Where

μ_i = Inlet flow viscosity, $kg\text{-}m^{-1}sec^{-1}$

ν_i = Inlet flow kinematic viscosity, m^2sec^{-1}

$C_{p,i}$ = Inlet flow heat capacity, $J\text{-}kg^{-1}\text{-}K^{-1}$

λ_i = Inlet flow thermal conductivity, $W\text{-}m^{-1}\text{-}K^{-1}$

The Inlet flow Reynolds number and the Prandtl number were then calculated.

$$Re_i = \sigma_i * (.01m/cm) * D_i * (1h/3600sec) * \nu_i^{-1} \quad (22)$$
$$Pr_i = C_{p,i} * \mu_i * \lambda_i^{-1} \quad (23)$$

Where

Re_i = Inlet Reynolds's number for ith section

Pr_i = Inlet Prandtl number for ith section

The change in pressure and temperature from the inlet to the outlet of each ith section is small enough to have a negligible effect on the values for the Reynolds number and Prandtl number. It was therefore assumed within the model that the Reynolds number and Prandtl number were constant within the ith section.

Based on the Reynolds number and the Prandtl number, the Nusselt number can be calculated. The equation used for the Nusselt number depends on the value of both the Reynolds number and the Prandtl number, and whether the flow is being heated or cooled [6],[7].

$$Nu_i = 3.657 \quad (24a)$$

for laminar flows with fully developed velocity and temperature profiles and Re < 2100. Likewise,

$$Nu_i = 0.024\, Re_i^{0.8}\, Pr_i^{0.4} \quad \text{for heating} \quad (24b)$$
$$= 0.026\, Re_i^{0.8}\, Pr_i^{0.4} \quad \text{for cooling} \quad (24c)$$

Where

Nu_i = Inlet Nusselt number for ith section

Equations (24b),(24c) are applicable for Re >2500 , $0.7 \le Pr \le 120$, and the length to diameter ratio of the flow channel is greater than 60.

From the Nusselt number, the heat transfer coefficient for the ith section can be calculated.

$$h_i = Nu_i * \lambda_i * D_i^{-1} * (100cm/m) \quad (25)$$

Where

h_i = ith section heat transfer coefficient, $W\text{-}m^{-2}\text{-}K^{-1}$

The heat transfer coefficient is assumed to be constant for the the ith section.

At this stage in the calculations the value of the inlet flow temperature of the (i + 1)th section is guessed and an iterative subroutine initiated. The first step in this iterative subroutine is the calculation of the average bulk flow temperature of the ith section.

$$T_{avg,i} = (T_i + T_{i+1})/2 \quad (26)$$

Where

$T_{avg,i}$ = Average bulk flow temperature, K

T_{i+1} = Inlet temperature of the (i + 1)th section, K

The average wall surface temperature of the ith section is calculated.

$$S_{avg,i} = (S_i + S_{i+1})/2 \quad (27)$$

Where

$S_{avg,i}$ = Average RGD/H wall surface temperature, K

S_{i+1} = (i + 1)th section wall surface temperature, K

Step 2 in the iterative subroutine calculates a heat transfer rate from the ith section based on the heat transfer coefficient.

$$Q_i = h_i * (0.0001\ m^2/cm^2)\ A_i * (T_{avg,i} - S_{avg,i}) \quad (28)$$

Where

Q_i = Heat transfer rate from ith section, W

Step 3 in the iterative subroutine calculates the parameters at the (i + 1)th position using the guessed value of T_{i+1} in place of T_i and equations (8), (9),(10), (11), and (12).

Step 4 in the iterative subroutine calculates the rate at which water has condensed or frozen onto the inner wall of the ith section of the RGD/H. This is calculated as the difference between the flow rate of water vapor at the ith section inlet and the (i +1)th section inlet.

$$\frac{\partial m_{l,i}}{\partial t} = \frac{\partial m_{w,i}}{\partial t} - \frac{\partial m_{w,i+1}}{\partial t} \quad (29)$$

Where

$\frac{\partial m_{l,i}}{\partial t}$ = Condensation rate in the ith section, kg/h

The inlet "dry gas" mass rate at the inlet of the (i+1)th section is the same as the mass rate at the inlet of the ith section.

$$\frac{\partial m_{g,i+1}}{\partial t} = \frac{\partial m_{g,i}}{\partial t} \quad (30)$$

Where

$\frac{\partial m_{g,i+1}}{\partial t}$ = Inlet dry gas mass rate to (i+1)th section, kg/h

Step 5 in the iterative subroutine calculates the enthalpy of the product gas, the water vapor, and the condensed water at both the ith position and the (i+1)th position. The enthalpy of the product gas, the water vapor, and the condensed water are functions of the inlet pressure and inlet temperature. Microsoft® Excel formulas were written for each of these enthalpies. These formulas were developed using enthalpy versus pressure and temperature data from references [3] and [5].

$$H_{g,i} = f_6(\text{product gas}, P_i, T_i) \quad (31)$$

$$H_{w,i} = f_7(\text{product gas}, P_i, T_i) \quad (32)$$

$$H_{l,i} = f_8(\text{product gas}, P_i, T_i) \quad (33)$$

$$H_{g,i+1} = f_6(\text{product gas}, P_{i+1}, T_{i+1}) \quad (34)$$

$$H_{w,i+1} = f_7(\text{product gas}, P_{i+1}, T_{i+1}) \quad (35)$$

Where

$H_{g,i}$ = Enthalpy of the ith section inlet product gas, Wh/kg

$H_{w,i}$ = Enthalpy of the ith section inlet water vapor, Wh/kg

$H_{l,i}$ = Enthalpy of the ith section condensate, Wh/kg

$H_{g,i+1}$ = Enthalpy of (i+1)th section inlet product gas, Wh/kg

$H_{w,i+1}$ = Enthalpy of (i+1)th section inlet water vapor,Wh/kg

Step 6 in the iterative subroutine is the calculation of a heat transfer rate from the ith section based on the guessed value of T_{i+1} and the change in enthalpies.

$$Q_{e,i} = H_{g,i}\frac{\partial m_{g,i}}{\partial t} + H_{w,i}\frac{\partial m_{w,i}}{\partial t} - H_{l,i}\frac{\partial m_{l,i}}{\partial t} - H_{g,i+1}\frac{\partial m_{g,i+1}}{\partial t} - H_{w,i+1}\frac{\partial m_{w,i}}{\partial t} \quad (36)$$

Where

$Q_{e,i}$ = Estimated heat transfer from ith section, Watt

Step 7 in the iterative subroutine is the comparison of the heat transfer calculated with equation (28) with the estimated heat transfer calculated with equation (36).

$$\Delta Q = Q_i - Q_{e,i} \quad (37)$$

Where

ΔQ = Heat transfer rate difference, W

If the heat transfer rate difference does not equal zero (or nearly zero), then a new guess for T_{i+1} must be made and steps 1 through 7 of the iterative subroutine repeated until the heat transfer rate difference, ΔQ, is equal to approximately zero. The Microsoft® Excel add-in subroutine program called SOLVER does the estimation and re-estimation of T_{i+1} automatically and ends with the final successful estimate of T_{i+1}.

With all the needed parameters calculated for the ith section, and the parameters determined for the (i+1)th position, the next short section is modeled. The (i+1)th parameters previously calculated are now used as inputs into the calculations for the (i+1)th short section, following the same procedure and equations as for the ith section. This process continues for each subsequent short section until all sections are modeled. This completes the modeling of the entire RGD/H.

Test Articles

A regenerative dryer test article was built to corroborate the analytical model with test data. The test article was designed to allow the formation and melting of the ice within the dryer to be viewed with a video camera from beneath the test article.

The test article is shown in figure 4. The test article consisted of a copper heat exchange surface that rejects heat to the ambient environment by a heat radiation process. Copper was chosen because its thermal conductivity is approximately the same as the carbon composite material used for the storage tanks. Attached to the interior of the heat exchange surface was an enclosed gas channel that was 61cm (24in) in length. The interior of the gas channel is viewable through the clear Lexan® cover. Attached to the interior of the heat exchange surface were foil heaters to simulate the heat absorbed from the fuel cell stack during operation of the regenerative fuel cell system. A supporting frame was attached to the test article to hold the shape of the test article and to allow the test article to be mounted in the test chamber. Figure 5 shows the test article on its supporting frame.

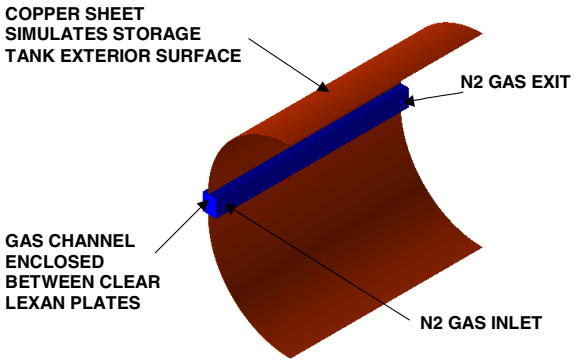

Figure 4.—RGD/H Test Article.

Additional testing was done with two commercially available; Department of Transportation (DOT) rated epoxy/fiberglass tanks. The tanks, which had seamless aluminum liners, were purchased from Carleton Technologies [8]. These tanks were modified by the addition of the RGD/H tubes as well as loop heat pipe (LHP) coils that were attached to the outside of each tank.

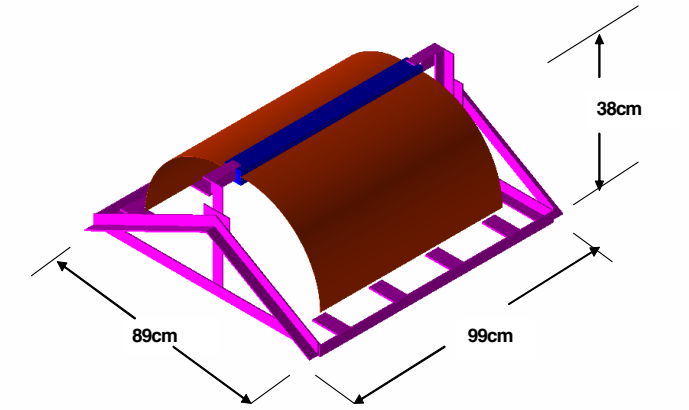

Figure 5.—RGD/H Test Article with Support Frame.

The RGD/H tubes and LHP coils were attached using Loctite 9394 epoxy [9] and the RS-3/K800 epoxy/carbon material [10]. The RS-3/K800 epoxy/carbon was used because of its high thermal conductivity, which is 391 W-m/K. The RS-3/K800 epoxy/carbon was applied in approximately 5cm (2in) strips that were run perpendicular to the heat pipes. Two overlapping layers (a total of 0.254cm (.010in) of thickness) of RS-3/K800 were applied in this fashion. One final strip of RS-3/K800 was applied directly over the RGD/H tube and LHP coils that was aligned in the same direction as the regenerative dryer tube and heat pipe. Figures 6 and 7 show the fabricated tanks.

The smaller of the two tanks, which represented the oxygen tank of a URFCS, was approximately 13.1 liters ($800in^3$) in volume with a diameter of 19.3cm (7.6in) and a length of 64.5cm (25.4in). Its weight before applying the epoxy/carbon was approximately 6.5kg (14.3 lbs). The RGD/H tube was 316SS tubing, 9.52mm (0.375in) OD and 0.89mm (.035in) wall thickness. The tubing was wrapped 1.5 turns (540° rotation) around the tank, and was approximately 106cm (41.8in) in length. Three and one third LHP coils were applied (approximately 208cm (82in) in length). The LHP tubing was 316SS, 2.54mm (0.1in) OD and 0.25mm (0.01in) wall thickness. The tank was wrapped with composite material over a surface area of approximately 0.40 m^2 for the oxygen tank.

The completed tank was shipped to Thermacore, Inc [11] for the addition of the LHP evaporator, compensation chamber, and other connective tubing. Thermacore, Inc charged the LHP with ammonia and did an initial check of the LHP operation before shipping the completed assembly to the NASA GRC. The completed assembly was instrumented with thermocouples and mounted within an aluminum frame (shown in Figure 6) for easy insertion into the thermal vacuum test chamber.

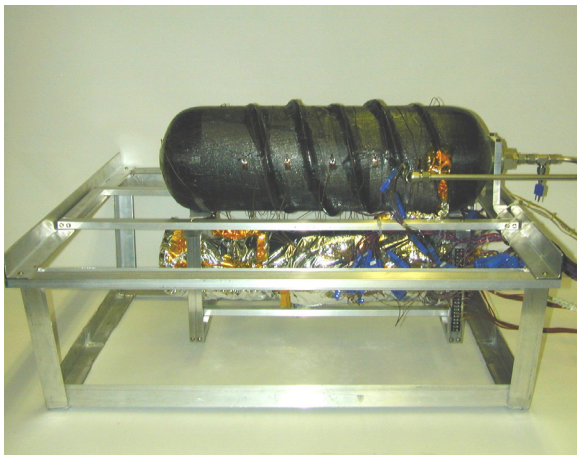

Figure 6.—Oxygen Tank with RGD/H and Heat Pipe.

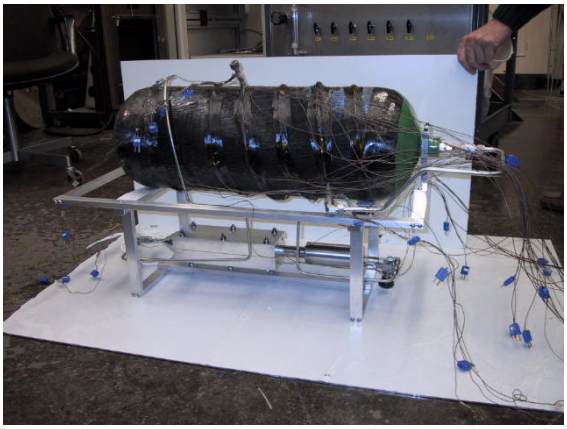

Figure 7.—Hydrogen Tank with RGD/H and Heat Pipe.

The larger of the two tanks, which represented the hydrogen tank of a URFCS, was approximately 24.6 liters (1500in^3) in volume with a diameter of 23.5cm (9.25in) and a length of 75.2cm (29.6in). Its weight before applying the epoxy/carbon was approximately 7.85kg (17.3lbs). The RGD/H tube was 316SS tubing, 9.52mm (0.375in) OD and 0.89mm (.035in) wall thickness. The tubing was wrapped 1.25 turns (450° rotation) around the tank, and was approximately 111cm (43.7in) in length. Three and one third LHP coils were applied (approximately 251cm (99in) in length). The LHP tubing was 316SS, 2.54mm (0.1in) OD and 0.254mm (0.01in) wall thickness. The tank was wrapped with composite material over a surface area of approximately 0.49 m^2 for the hydrogen tank. The larger tank was processed similarly to the smaller tank.

Experiments

Each of the experiments was conducted within a thermal vacuum chamber at NASA GRC. The vacuum chamber is cylindrically shaped with a 1 meter inside diameter and a length of about 1.5 meters. The vacuum chamber cold wall covered all interior surfaces of the chamber except the front access cover. The chamber was routinely operated at less than 10^{-6} Torr, and the cold wall was controlled at different environment temperatures form -30°C to -120°C.

The RGD/H test article was placed in the chamber with the long axis of the test article parallel to the long axis of the vacuum chamber as shown in Figure 8. A video camera, enclosed within its own environmental chamber was placed beneath the RGD/H test article to record images of the condensation and ice within the RGD/H channel during both the drying and rehumidification process. Dry, pre-heated nitrogen flowed through the camera enclosure to maintain the camera's temperature and to prevent fogging within the camera enclosure. The camera enclosure was able to be positioned anywhere along the length of the RGD/H by a motor drive and ball screw mechanism. Nitrogen gas that was used to simulate the hydrogen or oxygen gas in the URFCS, flowed through the RGD/H channel. The flow direction through the RGD/H was changed during the test to mimic the flow pattern expected during operation of the URFCS. An end view of the RGD/H test is shown in Figure 9. Temperatures were taken of the flowing gas at different positions along the RGD/H channel. Surface temperatures of the copper sheet were also recorded. The gas pressures at each end of the RGD/H channel were also recorded.

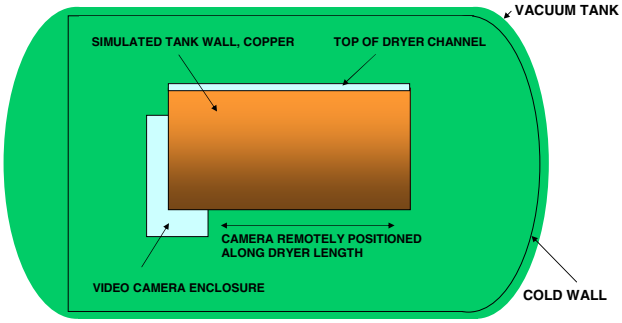

Figure 8.—Side View of RGD/H Test in Vacuum Chamber.

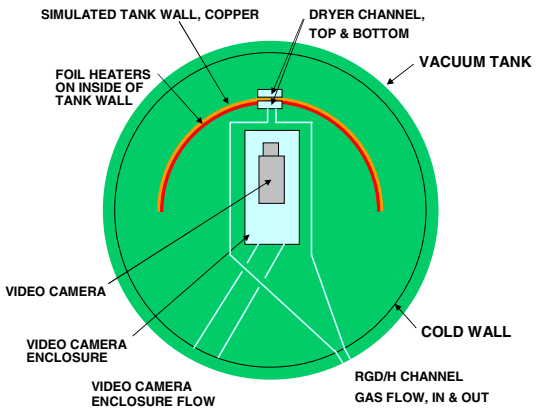

Figure 9.—End View of RGD/H Test in Vacuum Chamber.

Subsequent tests used the modified fiberglass/epoxy tanks previously described. Both tanks were inserted into the vacuum chamber and tested simultaneously. Rather than use oxygen and hydrogen for the testing, nitrogen was used to simulate oxygen and helium was used to simulate hydrogen. This was done to reduce safety concerns related to handling pressurized combustible gases.

The placement of each tank within the vacuum chamber is illustrated in Figure 10. Each tank was oriented with its long axis parallel to the long axis of the vacuum chamber. Electrical energy was supplied to the LHP evaporator that mimicked the waste heat produced by the operation of a URFC stack. The LHP system distributed this energy over the surface of each tank, and the RS-3/K800 carbon epoxy, acting as a heat fin, spread the heat over the surface of each tank.

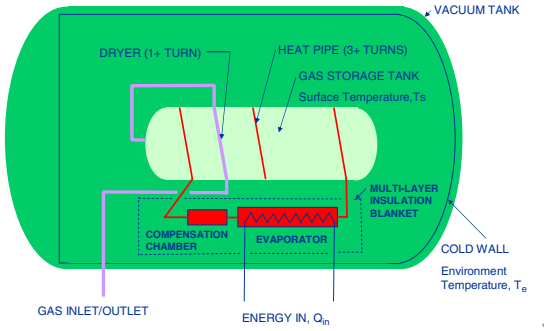

Figure 10.—O_2/H_2 Tank Placement in Vacuum Chamber.

Results – Regenerative Dryer Test Article

The test results from the testing of the copper RGD/H test article (the test article illustrated in Figure 4 and Figure 5) are shown in Figures 11, 12, 13, 14 and 15.

During the analysis of the data from the testing of the copper RGD/H it became apparent that the surface temperatures of the copper sheet did not accurately represent the wall temperatures of the RGD/H channel. Re-instrumentation of the test article was not feasible, and therefore the procedure for conducting the test was modified. In addition, an analytical methodology was developed to estimate the wall temperatures of the RGD/H channel. An example of how the test was conducted is shown in Figure 11. Figure 11 plots the flowing gas temperatures as a function of position along the RGD/H. Position "0" simulated the end of the RGD/H that was closest to the URFC stack exit and the position 61cm simulated the end of the RGD/H that was closest to the gas storage tank entrance. The data immediately before and after the switching of flow direction was plotted on the same graph. Figure 11 shows this for two instances during a test, one occurring at approximately 11:49AM and another at approximately 12:35PM. Since the time between the recorded data in each instance of flow direction switching was about 18 seconds, it was assumed that the channel wall temperatures did not appreciably change during the switching of the flow. It was also assumed that as the gas increases in temperature as it flows through the RGD/H , the wall temperature must be higher than the gas flow at each point along the RGD/H channel. Similarly, it was assumed that as the gas decreases in temperature as it flows through the RGD/H , the wall temperature must be lower than the gas flow at each point along the RGD/H channel. With these assumptions, the RGD/H wall temperature profile can be estimated as being between the curves representing the flow in each direction as shown in Figure 11.

The placement of the wall temperature profile between the switched flow curves was estimated by comparing the slope of each data curve at a given position. It was assumed that the shallower the slope of the data curve (ie the gas temperature is not appreciably changing) the closer the wall temperature must be to the temperature of the gas at that position. Similarly, the greater the slope of the data curve (ie the gas temperature is rapidly changing) the greater the difference must be between the wall temperature and the flowing gas temperature at a given position. Using these assumptions, the wall temperature profiles were estimated for each flow-switching instance. The estimated wall temperatures are shown on Figure 11.

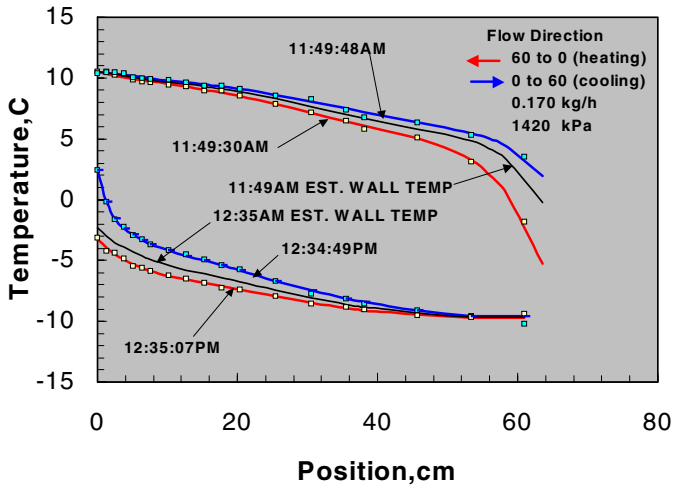

Figure 11.—RGD/H Thermal Profiles (Flow Switching).

Having estimated the wall temperatures of the RGD/H, these were entered into the Microsoft® Excel spreadsheet described earlier. In addition, the temperature of the gas at the flow entrance was also entered into the Microsoft® Excel spreadsheet. The model was then run, and the computed flowing gas temperature profile was compared to the actual measured temperature profile. Figure 12 shows these results for the data collected at 11:49:30.

Based on the mass flow, the channel flow dimensions, the temperature and pressure conditions, the calculated Reynolds number of the flow is less than 300, which would characterize the flow as laminar flow. When the heat transfer coefficient for laminar flow is used, the calculated temperature profile is not similar to the actual profile. If Equation (24b) is used, and the value of the Reynolds number used is 2000, the calculated temperature profile is very close to the measured temperature profile.

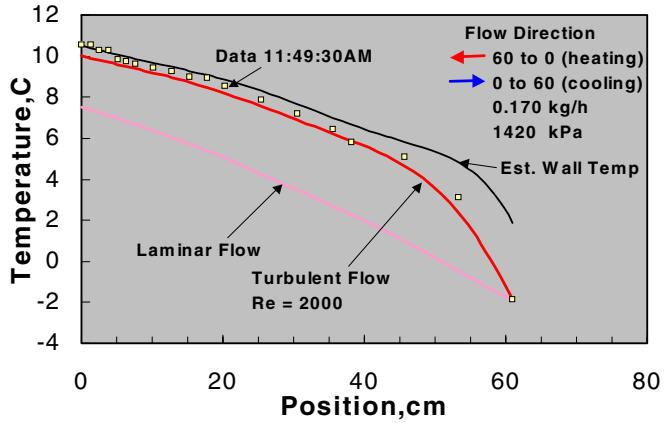

Figure 12.—Temperature Profile for 11:49:30 Data.

Figure 13 shows the results of the temperature profiles calculated for the data collected at 11:49:48. When the heat transfer coefficient for laminar flow is used, the calculated temperature profile is not similar to the actual profile. If Equation (24c) is used, and the value of the Reynolds number used is 2000, the calculated temperature profile is very close to the measured temperature profile. The results of Figure 13 are similar to that shown in Figure 12 in that the calculated profiles for laminar flow does not match the data, but if a Reynolds of 2000 is used the calculated profiles match the observed data for both flow directions.

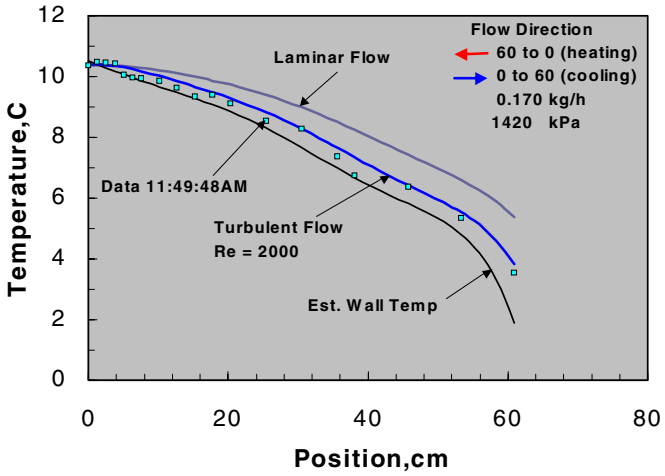

Figure 13.—Temperature Profile for 11:49:48 Data.

An analysis of the data collected at 12:34 is shown in Figures 14 and 15. The results of this analysis are similar to that shown in Figures 12 and 13. In each case the observed data does not match the calculated profiles for laminar flow, but instead match the calculated profiles when a Reynolds number of 2000 is used.

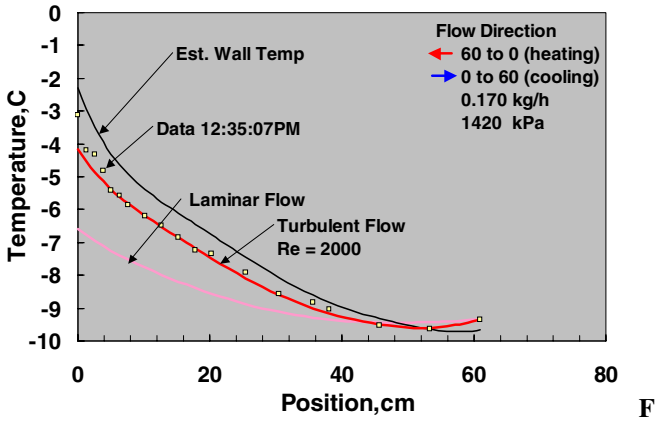

Figure 14.—Temperature Profile for 12:35:07 Data.

F

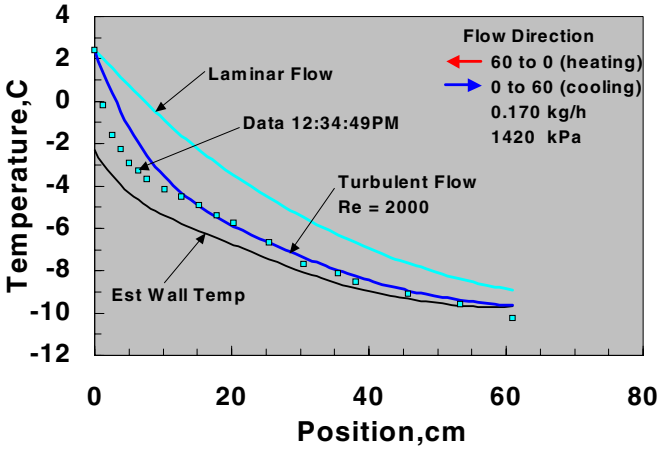

Figure 15.—Temperature Profile for 12:34:49 Data.

Data from other instances where the flow direction was switched were analyzed. These instances were deliberately set up to acquire data over a range of mass flow rates and pressures. For each instance the Reynolds number used to calculate the temperature profile was adjusted until the calculated results resembled the actual recorded temperature profiles. In all instances the resulting Reynolds number was a factor of 4 to 6 times greater than the Reynolds number calculated simply based on the mass flow, channel geometry, temperature and pressure conditions. One possible explanation for this is that the flow conditions are significantly more turbulent through the RGD/H channel than one would expect based on the calculated Reynolds number. The source of this increased turbulence could likely have been the thermocouple probes placed in the flow stream.

Figure 16 plots the heat transfer coefficient that resulted from a "best fit to the data" analysis as a function of pressure.

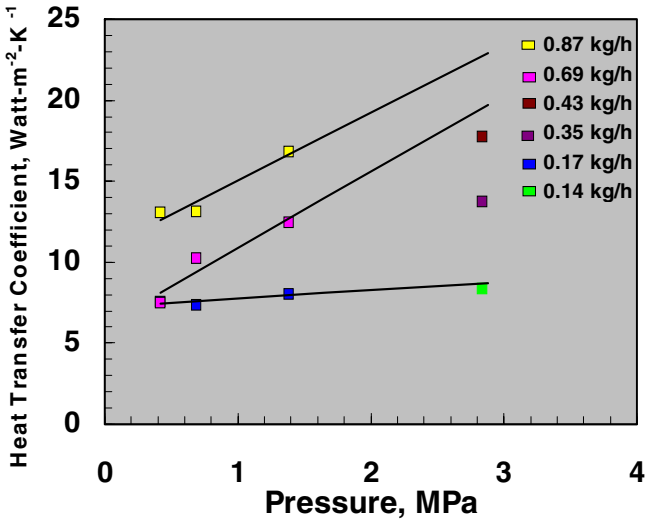

Figure 16.—Heat Transfer Coefficients versus Pressure.

It appears that for a given mass flow rate there is an increase in the heat transfer coefficient with increasing pressure, and that the slope of this increase becomes more pronounced with increasing mass flow rates.

It was also observed that the heat transfer coefficients at a given flow rate and at a given pressure were generally greater when the flow was being cooled than when the flow was being heated. Equations (24b) and (24c) allude to this since the Nusselt number is directly proportional to the heat transfer coefficient. The ratio of equation (24b) and (24c) results in the ratio of the cooling heat transfer coefficient to the heating heat transfer coefficient.

$$\frac{h_{i,cool}}{h_{i,heat}} = \frac{Nu_{i,cool}}{Nu_{i,heat}} = 0.026/0.024 = 1.083 \qquad (37)$$

Where

$h_{i,cool}$ = ith section cooling coefficient, watt-m^{-2}-K^{-1}

$h_{i,heat}$ = ith section heating coefficient, watt-m^{-2}-K^{-1}

$Nu_{i,cool}$ = ith section Nusselt number for cooling

$Nu_{i,heat}$ = ith section Nusselt number for heating

Figure 17 plots the ratios of the heat transfer coefficients that were calculated as part of the "best fit to the data" analysis. Figure 17 shows that the cooling heat transfer coefficient was consistently greater than the heating heat transfer coefficient by about the expected factor of 1.083. The precision of the measurements and the number of experiments done prevents any more quantitative assessment of this heat transfer coefficient ratio.

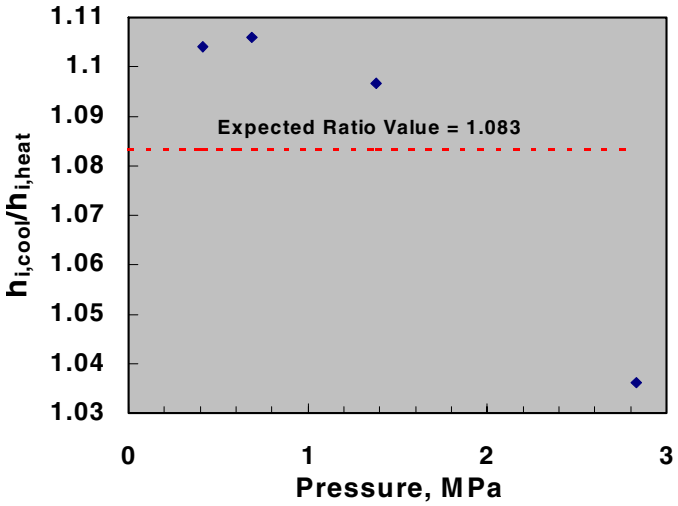

Figure 17.—Heat Transfer Coefficient Ratio vs. Pressure.

Results – Oxygen Tank Regenerative Dryer

Some of the results of the testing of the oxygen tank are shown in Figures 18 and 19. These results are representative of performance that was observed during the entire period of testing. Figure 18 shows the data obtained from the oxygen tank at 1:47:11PM July 22, 2004 along with the results obtained from the analytical model. The results show the temperature profile of both the wall of the dryer as well as the bulk flow as a function of position along the path length of the dryer. The results obtained with the oxygen tank are similar to that obtained with the Regenerative Dryer Test Article.

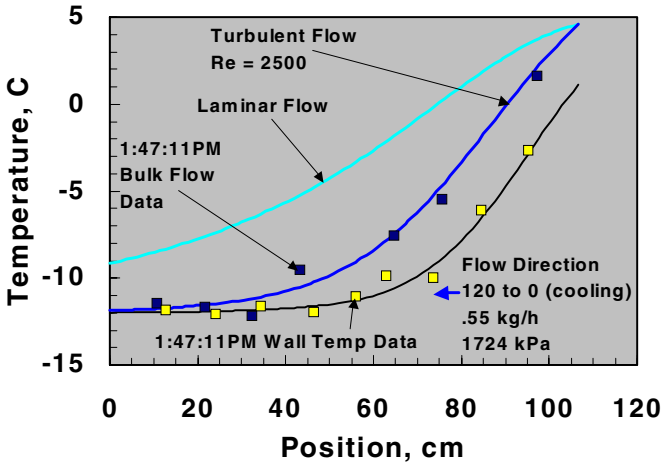

Figure 18.—Temperature Profile for 1:47:11PM Data.

The measured bulk flow temperature profile does not fit the bulk flow temperature profile based upon the calculated Reynolds number of 940 for this particular test, but if Equation (24c) is used with a value of 2500 for the Reynolds number, the model results closely resemble the measured

bulk temperature profile. The possible reason for this is the same as for the Regenerative Dryer Test Article, which is that the thermocouples placed in the tube to measure the flow temperature created turbulence that would not otherwise occur.

Figure 19 shows the data obtained from the oxygen tank at 2:45:40PM July 22, 2004 along with the results obtained from the analytical model. Like the results shown in Figure 18, the gas flow is being cooled. The calculated Reynolds number for this particular test was about 1300, which should also be laminar flow, but the model calculated temperature profile using this Reynolds number does not resemble the observed temperature profile. When Equation 24c is used with a Reynolds number value of 2500 the model calculated results do resemble the observed temperature profile.

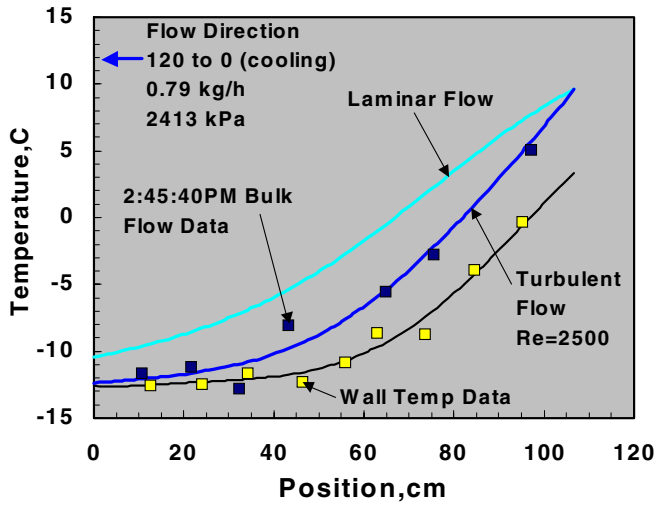

Figure 19.—Temperature Profile for 2:45:40PM Data.

Results – Hydrogen Tank Regenerative Dryer

Some of the results of the testing of the hydrogen tank are shown in Figures 20 and 21. These results are representative of performance that was observed during the entire period of testing. Figure 20 shows the data obtained from the hydrogen tank at 12:00:45PM July 22, 2004 along with the results obtained from the analytical model. The results show the temperature profile of both the wall of the dryer as well as the bulk flow as a function of position along the path length of the dryer. Unlike the results obtained with the previous tests, when the calculated Reynolds number of 90 is used, the model calculated results do resemble the observed temperature profile. The suggested reason for this is that helium was used in the test, and helium's thermal conductivity is much higher than the thermal conductivity of nitrogen, which was used in the oxygen tank test and the Regenerative Dryer test Article test. The thermal conductivity of helium is about six times that of nitrogen. Since the heat transfer coefficient is directly proportional to the thermal conductivity (see Equation 25), the heat transfer happens much quicker for the helium than for the nitrogen. As can be seen in Figure 20 the bulk gas flow temperature converges to the temperature of the dryer wall within the first 30 cm, whereas for the nitrogen, this convergence did not happen until the full length of the dryer. The effect of this quicker heat transfer is that it masks any effect of induced turbulence. The resolution and accuracy of the collected data is not sufficient to resolve temperature profile differences from any induced turbulence for the helium case.

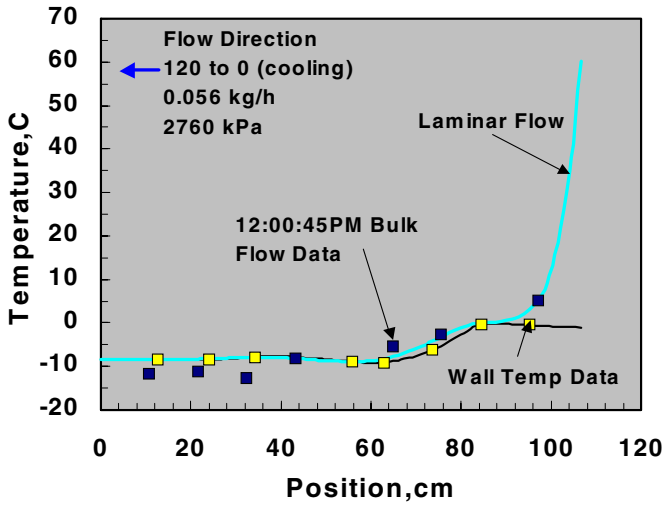

Figure 20.—Temperature Profile for 12:00:45PM Data.

Figure 21 shows the data obtained from the hydrogen tank at 2:45:40PM July 22, 2004 along with the results obtained from the analytical model.

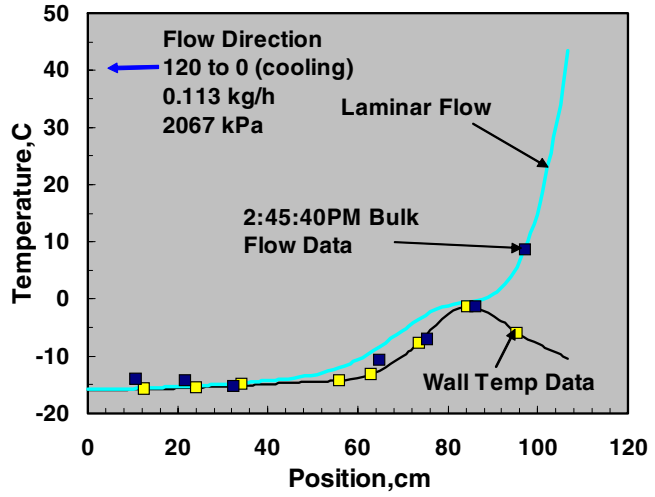

Figure 21.—Temperature Profile for 2:45:40PM Data.

The results show the temperature profile of both the wall of the dryer as well as the bulk flow as a function of position

along the path length of the dryer. These results are similar to that shown in Figure 20. The calculated Reynolds number for this test was 160-170. The temperature profile calculated by the model using this Reynolds number resembles the observed bulk flow temperature profile. The suggested reason for this is the same as for the results shown in Figure 20.

Conclusions

As stated earlier, the gas storage tanks, when used as heat radiating surfaces for the URFCS, cycle between freezing and thawing temperatures. The concept of the RGD/H wrapped around the outside of the gas storage tank to similarly cycle between freezing and thawing temperatures was tested and analyzed, and found to be a feasible solution to accomplish both the removal of moisture from the product gases as they are produced within the URFC stack as well as the re-humidification of the dry gases coming from the storage tanks and returning to the URFC stack.

The RGD/H analytical model proved a useful tool in attempting to understand the observed performance of the RGD/H, and with adjustment to account for induced turbulence, proved to be a reasonable predictor of the RGD/H performance. It would also be useful as a design tool for the future development of the RGD/H.

Based on the observed results as well as the results of the modeling, the following design considerations should be given to the future development of the RGD/H.

1) The RGD/H used in the oxygen stream should have a turbulence-generating device in order to reduce the overall length of this RGD/H.
2) The RGD/H used in the hydrogen stream can be much shorter in length than the RGD/H used in the oxygen stream because of hydrogen's higher thermal conductivity. Since the hydrogen flow is twice the oxygen flow there will be roughly twice the condensate/ice formed within the RGD/H. Provisions must be made to accommodate this condensate/ice formation within the shorter length so that the tubing does not become overly blocked, and flow restricted.

DEFINITIONS, ACRONYMS, AND ABBREVIATIONS

DC	Direct Current
DOT	Department of Transportation
FEA	Finite Element Analysis
GRC	Glenn Research Center
H_2	Hydrogen
LHP	Loop heat pipe
NASA	National Aeronautics and Space Administration
O_2	Oxygen
OD	Outside Diameter
RGD/H	Regenerative Gas Dryer/Humidifier
RFCS	Regenerative Fuel Cell System
URFC	Unitized Regenerative Fuel Cell
URFCS	Unitized Regenerative Fuel Cell System

A_i = Cross-sectional area, cm^2
$C_{p,i}$ = Inlet flow heat capacity, $J\text{-}g^{-1}\text{-}K^{-1}$
D_i = Hydraulic diameter of ith section, cm
h_i = ith section heat transfer coefficient, $W\text{-}m^{-2}\text{-}K^{-1}$
$h_{i,cool}$ = ith section cooling coefficient, $watt\text{-}m^{-2}\text{-}K^{-1}$
$h_{i,heat}$ = ith section heating coefficient, $watt\text{-}m^{-2}\text{-}K^{-1}$
$H_{g,i}$ = Enthapy of the ith section inlet product gas, Wh/kg
$H_{w,i}$ = Enthalpy of the ith section inlet water vapor, Wh/kg
$H_{l,i}$ = Enthalpy of the ith section condensate, Wh/kg
$H_{g,i+1}$ = Enthalpy of (i+1)th section inlet product gas, Wh/kg
$H_{w,i+1}$ = Enthalpy of (i+1)th section inlet water vapor,Wh/kg
λ_i = Inlet flow thermal conductivity, $W\text{-}m^{-1}\text{-}K^{-1}$
μ_i = Inlet flow viscosity, $g\text{-}cm^{-1}sec^{-1}$
$\frac{\partial m_{g,i}}{\partial t}$ = Inlet "dry gas" mass rate to ith section, kg/h
$\frac{\partial m_{g,i+1}}{\partial t}$ = Inlet dry gas mass rate to (i+1)th section, kg/h
$\frac{\partial m_i}{\partial t}$ = Inlet total mass flow rate, kg/h
$\frac{\partial m_{l,i}}{\partial t}$ = Condensation rate in the ith section, kg/h
$\frac{\partial m_{w,i}}{\partial t}$ = Inlet water vapor mass flow rate, kg/h
M_g = Molecular mass of the product gas, g/gmole
M_w = Molecular mass of water, g/gmole
Nu_i = Inlet Nusselt number for ith section
$Nu_{i,cool}$ = ith section Nusselt number for cooling
$Nu_{i,heat}$ = ith section Nusselt number for heating
$p_{g,i}$ = Inlet partial pressure of product gas, kPa
$p_{w,i}$ = Inlet partial pressure of water vapor, kPa
P_i = Inlet pressure of ith section, kPa
Pr_i = Inlet Prandtl number for ith section
ΔQ = Heat transfer rate difference, W

$Q_{e,i}$ = Estimated heat transfer from ith section, W
Q_i = Heat transfer rate from ith section, W
ρ_i = Inlet vapor mixture density, kg/m^3
R = 0.08205 atm-liter-$gmole^{-1}$- K^{-1}
Re_i = Inlet Reynolds number for ith section
σ_i = Inlet flow velocity of ith section, m/h
$S_{avg,i}$ = Average RGD/H wall surface temperature, K
S_i = Wall surface temperature of ith section, K
S_{i+1} = (i + 1)th section wall surface temperature, K
$T_{avg,i}$ = Average bulk flow temperature, K
T_i = Inlet flow temperature of ith section, K
T_{i+1} = Inlet temperature of the (i + 1)th section, K
ν_i = Inlet flow kinematic viscosity, m^2sec^{-1}
$\frac{\partial V_i}{\partial t}$ = Inlet volumetric flow rate, m^3/h
ΔX = Length of section, cm
X_i = Length to inlet of ith section, cm
$Y_{g,i}$ = Inlet mole fraction of product gas, %
$Y_{w,i}$ = Inlet mole fraction of water vapor, %

REFERENCES

[1] Burke, K.A. "Unitized Regenerative Fuel Cell System Development" NASA TM-2003-212739 and AIAA 1st International Energy Conversion Engineering Conference, August, 2003

[2] Burke, K.A. "Fuel Cells for Space Science Applications" NASA TM-2003-212730 and AIAA-2003-5938 presented at 2003 IECEC Conference

[3] Introduction to Thermodynamics: Classical and Statistical, Richard E. Sonntag, Gordon J. Van Wylen, Copyright 1971 John Wiley & Sons, Inc.

[4] Properties of Nonmetallic Fluid Elements, CINDAS Data Series on Material Properties Volume III-2, Edited by C.Y. Ho, Copyright 1989 Purdue Research Foundation, Published by Hemisphere Publishing Corporation

[5] Handbook of Physical Properties of Liquids and Gases Pure Substance and Mixtures, Third Augmented and Revised Edition, Natan B. Vargaftik, Yurii K. Vinogradov, Vadim S. Yargin, Copyright 1996 Begell House, Inc

[6] Handbook of Heat Transfer Third Edition, Warren M. Rohsenow, James P. Hartnett, Young I. Cho, Copyright 1998 McGraw Hill Companies, Inc.

[7] The CRC Handbook of Thermal Engineering, Edited by Frank Keith, Copyright 2000 CRC Press LLC

[8] Carleton Technologies Inc., 504 McCormick Drive, Glen Burnie, MD 21061

[9] Loctite Aerospace- Loctite Corporation 2850 Willow Pass Road P.O. Box 312 Bay Point, CA 94565-0031 Phone 925.458.8000

[10] Material obtained from Material Innovations Inc. 2200 Amapola Court, Suite 101 Torrance, CA 90501

[11] Thermacore Inc., 780 Eden Rd, Lancaster, PA 17601

REPORT DOCUMENTATION PAGE

Form Approved
OMB No. 0704-0188

1. AGENCY USE ONLY (*Leave blank*)	2. REPORT DATE	3. REPORT TYPE AND DATES COVERED
	October 2004	Technical Memorandum

4. TITLE AND SUBTITLE

Unitized Regenerative Fuel Cell System Gas Dryer/Humidifier Analytical Model Development

5. FUNDING NUMBERS

WBS–22–319–20–J1

6. AUTHOR(S)

Kenneth A. Burke and Ian Jakupca

7. PERFORMING ORGANIZATION NAME(S) AND ADDRESS(ES)

National Aeronautics and Space Administration
John H. Glenn Research Center at Lewis Field
Cleveland, Ohio 44135–3191

8. PERFORMING ORGANIZATION REPORT NUMBER

E–14823

9. SPONSORING/MONITORING AGENCY NAME(S) AND ADDRESS(ES)

National Aeronautics and Space Administration
Washington, DC 20546–0001

10. SPONSORING/MONITORING AGENCY REPORT NUMBER

NASA TM—2004-213355
AIAA–2004–5700

11. SUPPLEMENTARY NOTES

Prepared for the Second International Energy Conversion Engineering Conference sponsored by the American Institute of Aeronautics and Astronautics, Providence, Rhode Island, August 16–19, 2004. Kenneth A. Burke, NASA Glenn Research Center; and Ian Jakupca, Analex Corporation, Brook Park, Ohio 44142. Responsible person, Kenneth A. Burke, organization code 5420, 216–433–8308.

12a. DISTRIBUTION/AVAILABILITY STATEMENT

Unclassified - Unlimited
Subject Categories: 20 and 44 Distribution: Nonstandard

Available electronically at http://gltrs.grc.nasa.gov

This publication is available from the NASA Center for AeroSpace Information, 301–621–0390.

12b. DISTRIBUTION CODE

13. ABSTRACT ***(Maximum 200 words)***

A lightweight Unitized Regenerative Fuel Cell (URFC) Energy Storage System concept is being developed at the NASA Glenn Research Center (GRC). This Unitized Regenerative Fuel Cell System (URFCS) is unique in that it uses Regenerative Gas Dryers/Humidifiers (RGD/H) that are mounted on the surface of the gas storage tanks that act as the radiators for thermal control of the Unitized Regenerative Fuel Cell System (URFCS). As the gas storage tanks cool down during URFCS charging the RGD/H dry the hydrogen and oxygen gases produced by electrolysis. As the gas storage tanks heat up during URFCS discharging, the RGD/H humidify the hydrogen and oxygen gases used by the fuel cell. An analytical model was developed to simulate the URFCS RGD/H. The model is in the form of a Microsoft (registered trademark of Microsoft Corporation) Excel worksheet that allows the investigation of the RGD/H performance. Finite Element Analysis (FEA) modeling of the RGD/H and the gas storage tank wall was also done to analyze spatial temperature distribution within the RGD/H and the localized tank wall. Test results obtained from the testing of the RGD/H in a thermal vacuum environment were used to corroborate the analyses.

14. SUBJECT TERMS	15. NUMBER OF PAGES
Mathematical models; Fuel cells; Electrolysis; Temperature control; Energy storage; Regenerative fuel cells; Storage tanks; Drying apparatus	19
	16. PRICE CODE

17. SECURITY CLASSIFICATION OF REPORT	18. SECURITY CLASSIFICATION OF THIS PAGE	19. SECURITY CLASSIFICATION OF ABSTRACT	20. LIMITATION OF ABSTRACT
Unclassified	Unclassified	Unclassified	